J Fluoresc (2015) 25:1645–1654
DOI 10.1007/s10895-015-1651-9

ORIGINAL ARTICLE

Synthesis, Fluorescence Spectra, Redox Property and the DNA Binding Studies of 7-phenylacenaphtho[1,2-*b*]quinoxalin-7-ium chloride: Evidences of the Formation of Neutral Radical Analogue

Suman Kundu[1] · Ananya Banerjee[2] · Arpan De[2] · Asma Yasmeen Khan[3] · Gopinatha Suresh Kumar[3] · Ranjan Bhadra[1] · Prasanta Ghosh[1]

Received: 8 May 2015 / Accepted: 9 September 2015 / Published online: 23 September 2015

Abstract Reaction of acenaphthoquinone with *N*-phenyl-*o*-phenylenediamine in methanol in presence of HCl yielded 7-phenylacenaphtho[1,2-*b*]quinoxalin-7-ium chloride, [**1**][Cl]. [**1**][Cl] is brightly fluorescencent in dichloromethane (λ_{ex}= 403 nm and λ_{em}=442, 464, 488 nm) and water (λ_{ex}= 408 nm and λ_{em}=545 nm). Density functional theory (DFT) and time dependent (TD) DFT calculations on $[\mathbf{1}]^+$ at the B3LYP level of the theory elucidated that the origin of the lower energy excitation at around 400 nm is due to $\pi \rightarrow \pi^*$ transition. $[\mathbf{1}]^+$ is redox active and exhibits a reversible cathodic wave at −0.66 V referenced to Fc^+/Fc couple due to $[\mathbf{1}]^+/[\mathbf{1}]^\bullet$ redox couple. Electrogenerated neutral radical analogue $[\mathbf{1}]^\bullet$ was characterized by electron paramagnetic resonance (EPR), UV–vis spectra and DFT calculations. DNA binding studies using the techniques of UV–vis absorption, fluorescence, circular dichroism (CD) spectra, viscosity, gel electrophoresis, hydrodynamic, isothermal titration calorimetry (ITC) and UV optical melting studies of [**1**][Cl] revealed that $[\mathbf{1}]^+$ is a strong DNA intercalator obeying neighbor exclusion principle. ITC experiment authenticated that the binding of $[\mathbf{1}]^+$ to DNA is entropy driven.

Keywords 7-phenylacenaphtho[1,2-*b*]quinoxalin-7-ium chloride · 7-phenylacenaphtho[1,2-*b*]quinoxalin radical · DNA intercalator · Biophysical studies

Introduction

Small organic cations those can bind and intercalate DNA are significant and considered as potential therapeutic agents [1–12]. These cations can be treated as cell cycle abrogators by virtue of arresting the DNA replication. Ethidium bromide is a well established strong intercalator of DNA, but not complying with safety to use in therapy. Heterocycles resembling ethidium bromide (EB) and behaving similarly with safety compliance may be considered of high drug value. The planar organic cations those resemble EB are not common in literature [13]. The planar cationic transition metal complexes are rather common. However, the cytotoxicities of the transition metal ions in many cases are alarming [14]. In this project we were persuaded to develop organic cations and study their DNA intercalation property. Recently we reported 9-phenyldibenzo[*a,c*]phenazin-9-ium cation [15], the geometrical feature of which is similar to that of ethidium bromide, as depicted in Chart 1, as a strong DNA intercalator [15]. However, the poor solubility of it in water hindered its use in biological applications. In this article, we report another organic cation, 7-phenylacenaphtho[1,2-*b*]quinoxalin-7-ium chloride, [**1**][Cl] as depicted in Chart 1, which is soluble in water, redox active and fluorescent in fluid solution.

The formation of the neutral 7-phenylacenaphtho[1,2-*b*-]quinoxalin, $[\mathbf{1}]^\bullet$ radical analogue upon reduction of $[\mathbf{1}]^+$ ion is substantiated by spectroelectrochemical measurements,

Electronic supplementary material The online version of this article (doi:10.1007/s10895-015-1651-9) contains supplementary material, which is available to authorized users.

✉ Prasanta Ghosh
ghosh@pghosh.in

[1] Department of Chemistry, R. K. M. Residential College, Narendrapur, Kolkata 700103, India

[2] VJRC R&D Center, Vijaygarh Jyotish Ray College, Bijoygarh, Kolkata 700 032, India

[3] Biophysical Chemistry Laboratory, Organic and Medicinal Chemistry Division, CSIR-Indian Institute of Chemical Biology, Kolkata 700032, India

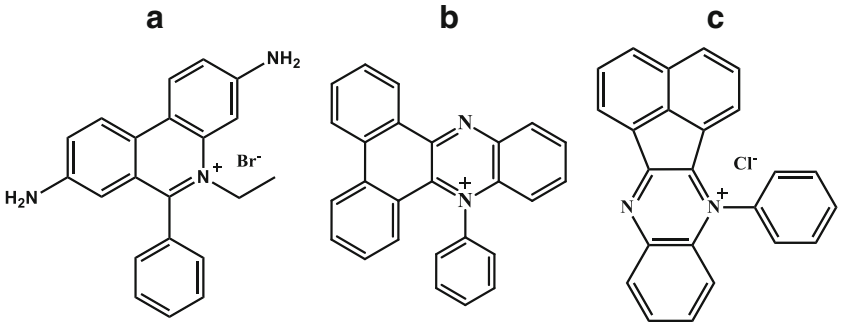

Chart 1 Structure of **a** ethidium bromide, **b** 9-phenyldibenzo[*a,c*]phenazin-9-ium and **c** 7-phenylacenaphtho[1,2-*b*]quinoxalin-7-ium chloride [**1**][Cl]

EPR spectra and density functional theory (DFT) calculations. UV–vis absorption spectra, fluorescence spectral study, circular dichroism, viscosity, gel electrophoresis, hydrodynamic, isothermal titration calorimetry and UVoptical melting studies of [**1**][Cl] authenticates that $[\mathbf{1}]^+$ ion is a strong DNA intercalator.

Materials and Methods

Calf thymus DNA (CT DNA, Type I, 42 % GC content) and other reagents were obtained from Sigma-Aldrich Corporation (MO, USA) and used without further purification. The DNA solution was freshly made in the buffer and concentration was determined by taking molar absorption coefficient (ε) 13, 200 $M^{-1}cm^{-1}$. The 260/280 nm ratio of absorption of DNA solution was about 1.8 indicating the sample to be free from contaminating proteins. [**1**][Cl] molecule was soluble in the buffer and its concentration was determined at 338 nm using a ε value of 53,400 M^{-1} cm^{-1}. Spectroscopic grade solvents were used for spectral measurements. The C, H, N contents of the compounds were obtained from Perkin-Elmer 2400 series II elemental analyzer. Infrared spectra of the samples were measured from 4000 to 400 cm^{-1} as KBr pellets at room temperature on a PerkinElmer FT-IR-Spectrophotometer Spectrum RX1. ^{1}H NMR spectral measurements were carried out on a Bruker DPX-300 MHz spectrometer with tetramethylsilane (TMS) as an internal reference. ESI mass spectra were recorded on a micro mass Q-TOF mass spectrometer. Electronic absorption spectra in solution at 25 °C were measured on a PerkinElmer Lambda 25 spectrophotometer in the range 200–1100 nm. Fluorescence data and fluorescence quenching studies were recorded on a PerkinElmer LS 55 fluorescence spectrophotometer. The electro analytical instrument, BASi Epsilon-EC for cyclic voltammetric experiment in CH_2Cl_2 solutions containing 0.2 M tetrabutylammonium hexafluorophosphate as supporting electrolyte was used. The BASi platinum working electrode, platinum auxiliary electrode, Ag/AgCl reference electrode were used for the measurements. The redox potential data are referenced vs. ferrocenium/ferrocene, Fc^+/Fc, couple. BASi SEC-C thin layer quartz glass spectroelectrochemical cell kit (light path length of 1 mm) with platinum gauze working electrode and SEC-C platinum counter electrode were used for spectroelectrochemistry measurements. The X-band EPR spectra were measured on Magnettech GmbH MiniScope MS400 EPR spectrometer. DNA binding studies were performed on a Jasco V660 spectrophotometer. Cannon-Manning semi micro size 75 capillary viscometer (Cannon Instrument Company, State College, PA, USA) was used for measuring the flow times. Circular dichroism spectra were recorded in a PC-controlled Jasco J815 model spectropolarimeter (Jasco International Co. Ltd., Hachioji, Japan) equipped with a temperature controller (Jasco model PFD

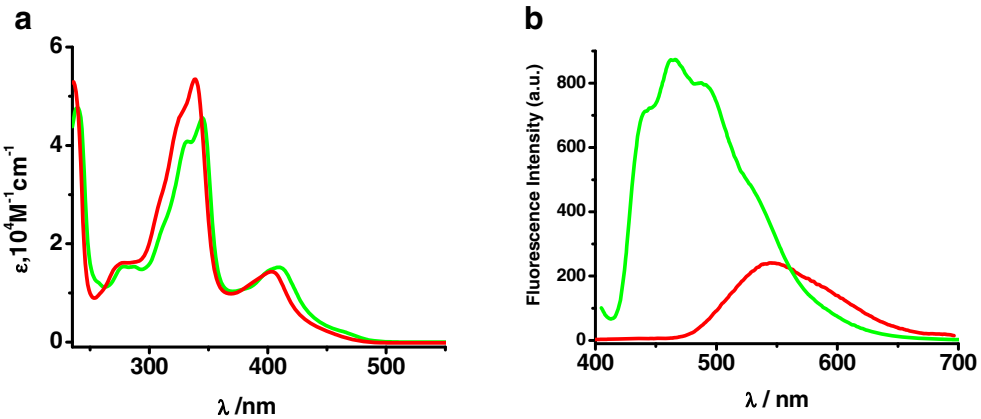

Fig. 1 **a** UV–vis spectra of [**1**][Cl] in CH_2Cl_2 (*green*) and buffer (*red*) and **b** emission spectra of [**1**][Cl] in CH_2Cl_2 (*green*) and buffer solution (pH= 7.2) (*red*) at 25 °C

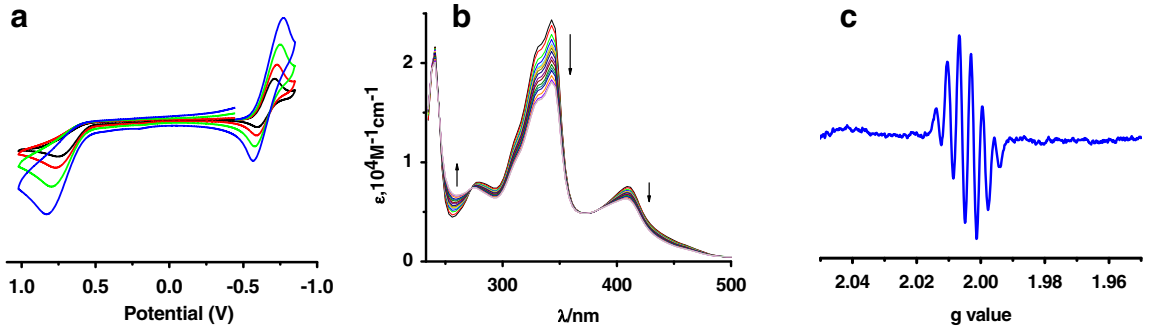

Fig. 2 **a** Cyclic voltammogram of [**1**][Cl] in CH_2Cl_2 at 25 °C (Conditions: 0.2 M $[N(n\text{-}Bu)_4]PF_6$ supporting electrolyte; scan rate, 50 (*black*), 100 (*red*), 200 (*green*) and 400 (*blue*) mv s^{-1}; platinum working electrode). **b** Spectroelectrochemistry of $[\mathbf{1}]^+$ to $[\mathbf{1}]^\bullet$ in CH_2Cl_2 solution at 25 °C. **c** EPR spectrum of the electrogenerated $[\mathbf{1}]^\bullet$ in CH_2Cl_2 at 25 °C

425 L/15) at 20±0.5 °C in the wavelength range 200–400 nm. Isothermal titration calorimetric (ITC) experiments were performed at 20 °C using a MicroCal VP-ITC unit (MicroCal LLC, Northampton, MA, USA). Thermal melting curves of DNA-drug complexes were measured on the Shimadzu Pharmaspec uv-1700 unit equipped with the Peltier-controlled TMSPC-8 model accessory (Shimadzu Corporation, Kyoto, Japan). Gel documentation was performed by BIO-RAD Gel Electrophoresis and Documentation System (BIO-RAD Pacific Ltd., Hong Kong). Origin 7.0 software, (Origin Lab. Corporation, Northampton, MA, USA), was used for data acquisition and analysis.

Synthesis

[1][Cl] To acenaphthoquinone (182 mg, 1.0 mmol) in methanol (50 mL), *N*-phenyl-*o*-phenylenediamine (184 mg, 1.0 mmol) and few drops of concentrated HCl were added successively and the reaction mixture was refluxed for 45 min (at 65 °C). The reaction mixture was cooled at room temperature and filtered. The solution was allowed to evaporate slowly at room temperature (25 °C). After a few days, yellow micro crystals of [**1**][Cl] separated out, which are collected upon filtration and dried in air. Yield: 310 mg (~85 % with respect to acenaphthoquinone). ESI (positive ion)-MS in CH_3CN; *m/z*: 331.20 for $[\mathbf{1}]^+$. Anal. Calcd. for $C_{24}H_{15}ClN_2$: C, 78.58; H, 4.12; N, 7.64; Found: C, 78.35; H, 4.15; N, 7.55. ^1H NMR ($CDCl_3$, 300 MHz, 25 °C) δ (ppm)=9.44 (t, 1H), 8.79 (d, 2H), 8.58 (d, 2H), 8.38 (d, 2H), 8.25 (d, 2H), 7.98 (m, 3H), 7.62 (t, 2H), 7.32 (t, 1H). IR (KBr, ν_{max}/cm^{-1})=3422(s), 3020(m), 1600(s), 1438(m), 1421(m), 1320(s), 1111(vs), 1040(m), 770(s), 598(m), 552(s).

Density Functional Theory (DFT) Calculations

All calculations reported in this article were done with the Gaussian 03 W [16] programme package supported by GaussView 4.1. The DFT [17–20] and TD DFT [21–23] calculations were performed at the level of Becke three parameter hybrid functional with the non-local correlation functional of Lee-Yang-Parr (B3LYP) [24–26]. The geometries of $[\mathbf{1}]^+$ and $[\mathbf{1}]^\bullet$ in gas phase were optimized using Pulay's Direct Inversion [27] in the Iterative Subspace (DIIS), 'tight' convergent SCF procedure ignoring symmetry [28]. In all calculation, a 6-31G^{++} (d, p) basis set was used [29, 30]. The 60 lowest singlet excitation energies on the optimized geometry of $[\mathbf{1}]^+$ in dichloromethane were calculated by TD DFT method using conductor-like polarizable continuum model (CPCM) [31,

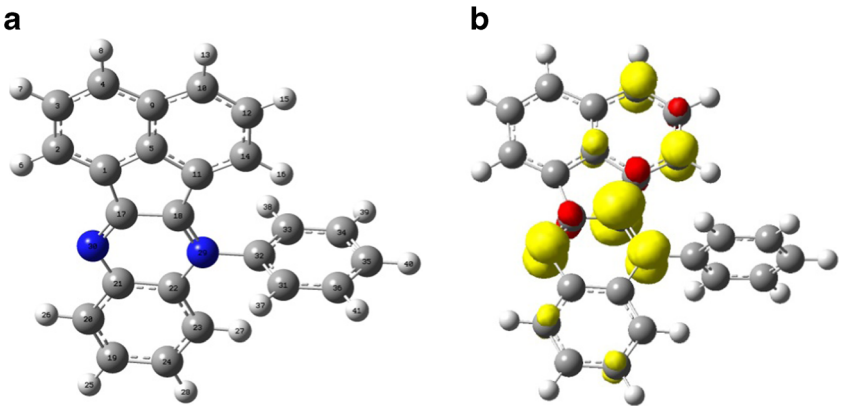

Fig. 3 **a** Gas phase optimized geometry of $[\mathbf{1}]^+$ and **b** atomic spin densities of $[\mathbf{1}]^\bullet$ (*yellow*, α spin; *red*, β spin) and atomic spin densities obtained from Mulliken spin population analyses (spin density, C10 0.17, C14 0.18, C18 0.38, N29 0.17, N30 0.26)

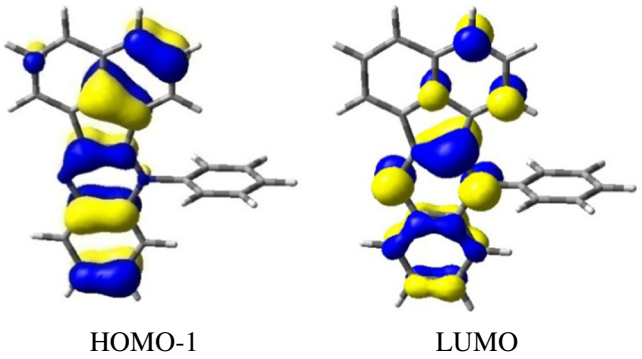

Fig. 4 Photoactive orbitals of $[\mathbf{1}]^+$ ion

32]. The nature of transitions was calculated by adding the probability of same type among the molecular orbitals.

DNA Binding Studies

DNA binding experiments were performed in 10 mM Tris–HCl, pH 7.0±0.2 containing 50 mM NaCl. The planar heteroaromatic [**1**][Cl] molecule was soluble in the buffer and its organic cation $[\mathbf{1}]^+$ was stable.

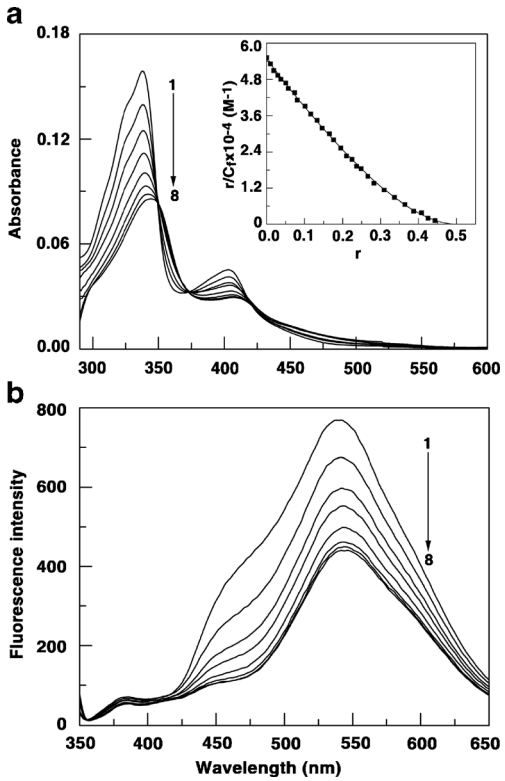

Fig. 5 **a** Absorbance spectra of [**1**][Cl] (11 μM) treated with 0, 5.5, 11.0, 16.5, 27.5, 44.0, 55.0 and 77.0 μM of CT DNA (Curves 1–8). The inset shows the Scatchard plot of the binding. **b** Fluorescence titration data on constant amount of [**1**][Cl] by CT-DNA (curves 1–8). The excitation wavelength was 408 nm

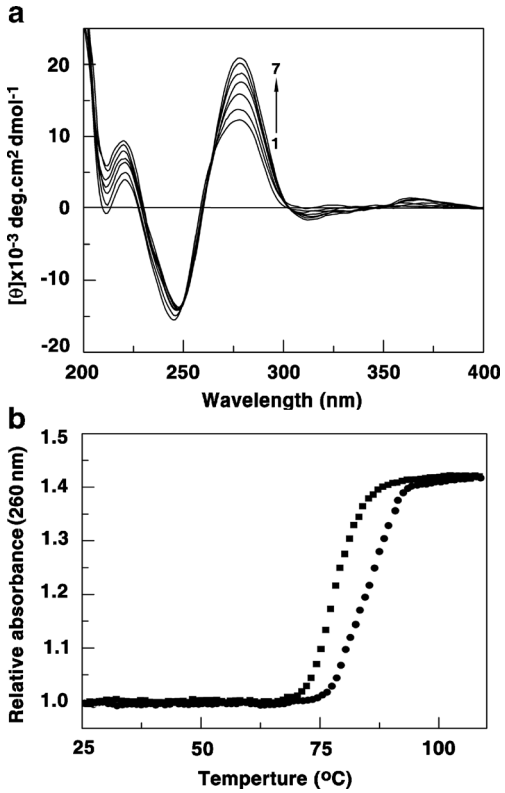

Fig. 6 **a** CD-spectra resulting from the interaction of [**1**][Cl] with DNA. Curves 1→7 denote the interaction of CT DNA (60 μM) treated with 0, 6, 12, 18, 30, 42 and 60 μM of [**1**][Cl]. **b** Thermal melting profiles of DNA (20 μM) (*black square*) treated with [**1**][Cl] (*black circle*) at a drug/base pair molar ratio of 1.3

UV–vis Spectroscopy

A same amount of DNA was taken in the buffer both in the sample and reference cuvettes maintained at 20±1 °C. It was then titrated with the increasing concentration of [**1**][Cl] solution with constant stirring. Briefly, after each addition of the aliquot of [**1**][Cl] solution to the DNA the absorbance was recorded after allowing about 2 min to re-equilibrate. The isosbestic point at 349 nm for [**1**][Cl] was determined and concentration of total bound of [**1**][Cl] was calculated. The absorbance at the isosbestic point 349 (λ_{iso}) and wavelength maximum (λ_{max}) of the cation $[\mathbf{1}]^+$ were determined after each addition. The absorption extinction coefficient of [**1**][Cl] at the isosbestic point (ε_{iso}) was determined and the extinction coefficient of bound [**1**][Cl] (ε_B) was obtained by addition of a known quantity of [**1**][Cl] to a large excess of DNA corresponding to the saturation point: $(\varepsilon_B)=A_{max}/lC_t$ where l is the path length and C_t is total [**1**][Cl] concentration present that was calculated as $C_t=A_{iso}/l\varepsilon_{iso}$. The values of A_{max}, A_{iso}, ε_{iso}, and ε_B were determined and these are used to calculate the expected absorbance at the wave length maximum as, $A_{exp}=lC_t\varepsilon_{max}$, where ε_{max} is the molar absorption coefficient at the wavelength maxima. The difference in A_{exp} and observed absorbance was used to calculate the amount of bound

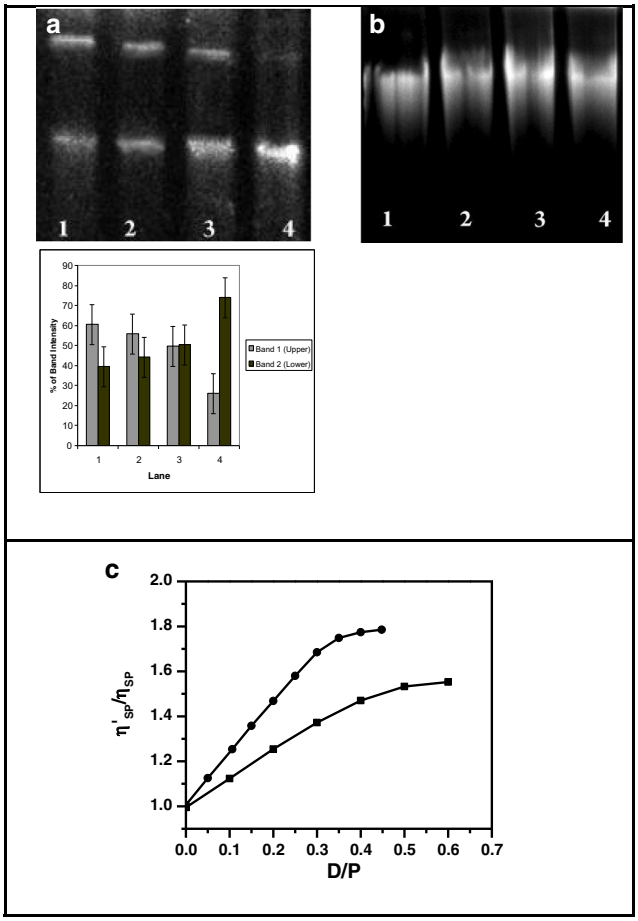

Fig. 7 Changes in electrophoretic mobility pattern of pUC19 DNA and CT DNA in the agarose gel (in panel **a** the upper panel indicates the band positions, while the lower panel shows band intensity). Lane 4 of panel **a** and Lane 1 in panel **b** display pUC19 DNA and CT DNA (untreated), respectively. Lanes 3, 2 and 1 of panel **a** and lanes 2, 3 and 4 of panel **b** indicate treated DNA using doses of 4.0, 6.0 and 8.0 mM of [**1**][Cl]. **c** Plot of change in relative viscosity of DNA (250 μM) with increasing concentrations of [**1**][Cl] (-■-). The standard curve for ethidium bromide is also shown (-●-)

[**1**][Cl]. The concentrations of free (C_f), bound (C_b) and total (C_t) of [**1**][Cl] were determined [33]. The binding data were used to construct Scatchard plots of r/C_f vs. r, where r is the number of moles of [**1**][Cl] bound per mole of DNA base pair and C_f the molar concentration of free [**1**][Cl]. The binding isotherms were analyzed according to the excluded site model of McGhee and von Hippel for nonlinear non-cooperative ligand binding system using the following equation: [34]

$$\frac{r}{C_f} = K_i(1-nr)\left[\frac{(1-nr)}{\{1-(n-1)r\}}\right]^{(n-1)}$$

where K_i is the intrinsic binding constant to an isolated site and n is the number of base pair excluded by the binding of a single [**1**][Cl] molecules. The binding data were analysed using Origin software to determine the best fit parameters of K_i and n to be the above equation [35].

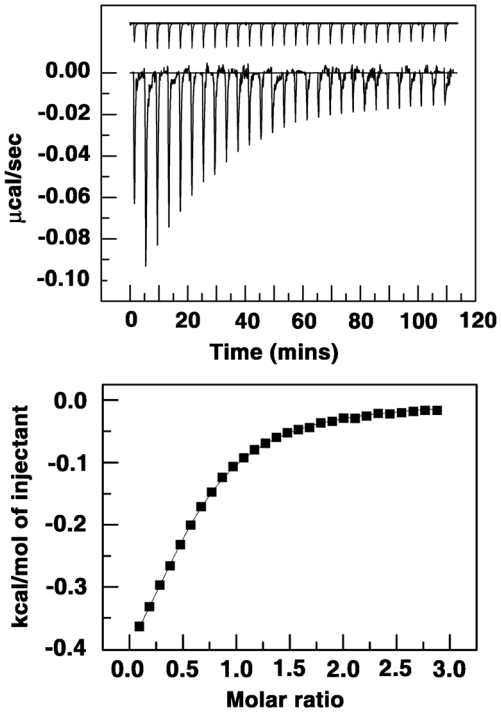

Fig. 8 ITC profile for the titration of [**1**][Cl] into a solution of CT DNA at 20 °C. Top panel of the figure represents plots of enthalpy against time representing the raw data for the sequential injection of [**1**][Cl] (800 μM) into DNA (60 μM), solution and dilution of [**1**][Cl] into buffer (curves on the top offset for clarity). In the corresponding lower panels, plots of enthalpy against mole ratio showing the integrated heat results after correction of heat of dilution against the mole ratio of [**1**][Cl]/DNA is presented. The data points (*closed squares*) were fitted to a one-site model and the solid lines represent the best-fit results

Fluorescence Emission Spectral Study

[**1**][Cl] exhibits strong emission bands in the range of 500–600 nm when excited at 408 nm. The 1 cm path length quartz cuvette was filled with buffer (2.5 mL) and examined for fluorescence emission after addition of [**1**][Cl] or DNA. The DNA concentration to quench the fluorescence of [**1**][Cl] more than 50 % was determined by titration.

Circular Dichroism Spectroscopy

Titrations were performed at 20±1 °C by addition of increasing concentrations of [**1**][Cl] to a fixed concentration of CT DNA (60 μM) taken in the cuvette of 1 cm path length. Each spectrum was averaged from four successive accumulations and was baseline corrected and smoothed within the permissible limits using the Jasco software of the unit. The following settings were used for spectral accumulations; scan rates 50 nm min^{-1}; bandwidth 1 nm; sensitivity, 100 millidegrees. The molar ellipticity values [θ] were calculated from the equation $[\theta]=100\times\theta/(C\times l)$, where θ is the observed ellipticity in millidegrees, C is the concentration in moles/lit, and l is the

cell path length of the cuvette in cm. The molar ellipticity [θ] (deg.cm^2/dmol) values are expressed in terms of base pairs in the region 200–400 nm.

Hydrodynamic Studies

The viscosity of the DNA-[**1**][Cl] complexes was determined by measuring the time of flow through the viscometer that was immersed in a thermostated water bath maintained at 20± 1 °C. Flow times of DNA alone (sonicated to 2.0–2.5× 10^5 Da) and with different ratios of [**1**][Cl] were measured in triplicate by an electronic stopwatch with an accuracy of ±0.01 s. The flow time $t_{control}$, $t_{complex}$ and t_0 were determined for DNA, DNA-[**1**][Cl] complex and buffer alone by averaging six reading for each. Relative viscosity of various sets was calculated from the relation, $\eta'_{sp}/\eta_{sp} = \{(t_{complex} - t_0)/t_0\}/\{(t_{control} - t_0)/t_0\}$ where η'_{sp} and η_{sp} are specific viscosity of the DNA-[**1**][Cl] complex and DNA alone, respectively [36].

Gel Eelectrophoresis

The interaction of [**1**][Cl] with pUC19 plasmid DNA (250 ng) and CT DNA (500 ng) was studied by agarose gel electrophoresis. pUC19 DNA isolated from *E. coli* DH5α by Alkaline Lysis method and sonicated CT DNA were incubated with various concentrations of drug [**1**][Cl] (4.0, 6.0 and 8.0 mM) for 2.5 h at 37 °C and loaded in 1 % agarose gel in TAE buffer (pH 8.0) at a current of 2 V/cm (for pUC 19 DNA) and 3 V/cm (for CT DNA) for 4 h [15].

Isothermal Titration Calorimetry (ITC) Experiments

In this experiment, aliquots of a 800 μM [**1**][Cl] solution were injected from a 250 μL rotating syringe (290 rpm) into the isothermal sample chamber containing 1.4235 mL of 60 μM DNA solution. Corresponding control experiments were performed to determine the heat of dilution of [**1**][Cl] to buffer. Before use, all the solutions were degassed under vacuum (140 mbar, 8 min) on the Thermovac to eliminate air bubble formation inside the calorimeter cell. The duration of each injection was set at 10 s and the delay time between each injection was 300 s. Each injection generated a heat spike curve (micro calories per second vs. time) the intensity of which reduced as saturation in the binding approached. The area under each peak was determined by integration using the software to give the measure of the heat associated with the injection. The heat associated with each drug-buffer titration (control heat) was subtracted from the corresponding heat associated with each [**1**][Cl]-DNA injection to give the heat of binding for that injection. The resulting corrected injection heats were plotted as a function of molar ratio and fit with a model for one set of binding sites. Analyzed by Origin 7.0 the thermodynamic parameters of the binding, the binding affinity (K_a), the binding stoichiometry (n), the enthalpy of binding (ΔH^o), binding Gibbs energy (ΔG^o) and the entropic contribution ($T\Delta S^o$) to the binding.

UV Optical Melting Study

Thermal melting profiles of [**1**][Cl]-DNA complexes were measured. The DNA was mixed with varying concentrations of [**1**][Cl] in degassed buffer in micro-optical cuvettes of 1 cm path length and the temperature of the cuvette assembly was raised from 20 to 110 °C at a rate of 0.5 °C min^{-1}, by continuously registering the absorbance change at 260 nm. From the melting curves the melting temperature T_m as revealed from the midpoint temperature of the [**1**][Cl] bound DNA unfolding process and the hyperchromicity changes were obtained. The T_m value is reproducible to within ±1 °C.

Results and Discussion

Syntheses and Characterization

The yellow crystalline compound [**1**][Cl] was isolated in good yields from a reaction of acenaphthoquinone and *N*-phenyl-*o*-phenylenediamine in presence of catalytic amount of concentrated HCl in methanol. The molecular composition of the cation was confirmed by the elemental analyses and ESI (+ve) mass spectrum. No NH bond was detected in the IR spectrum of [**1**][Cl]. The UV–vis absorption spectra of [**1**][Cl] in dichloromethane and buffer at pH 7.2 were recorded and are shown in Fig. 1a. The absorption spectral data are summarized in Table 1. The cation absorbs strongly at 410 and 344 nm.

Fluorescence Spectra

[**1**][Cl] is emissive in CH_2Cl_2 and buffer solutions. The emission spectra were recorded upon exciting at 408 and 403 nm (Table 1). The emission spectra are shown in Fig. 1b. The emission band of the cation in CH_2Cl_2 is structured and is blue shifted compared to these in buffer solution.

Redox Series and EPR Spectra

The redox activity of $[\mathbf{1}]^+$ ion to assess the stability of the corresponding electrogenerated neutral $[\mathbf{1}]^\bullet$ species in solution was studied by cyclic voltammetry in CH_2Cl_2 containing 0.2 M tetrabutylammonium hexafluorophosphate as supporting electrolyte at 25 °C. The experiments were

Table 1 UV–vis absorption, excitation (λ_{ex}) and emission (λ_{em}) spectral data of [**1**][Cl] in CH_2Cl_2 and buffer solution (pH=7.2) at 25 °C

Solvent	λ_{max}, nm (ε,10^4 $M^{-1}cm^{-1}$)	λ_{ex}, nm	λ_{em}, nm
CH_2Cl_2	410(1.53), 344(4.55), 330(4.14) 287(1.55), 277(1.55), 238(4.74)	403	442, 464, 488
Buffer	404(1.43), 338(5.34), 326(4.65) 274(1.60), 237(5.25)	408	545

performed with different scan rates. The redox potential data were referenced to ferrocenium/ferrocene, Fc^+/Fc, couple. The cyclic voltammogram of [**1**][Cl] is illustrated in Fig. 2a. No reversible anodic wave was detected. The irreversible anodic peak with $E_{½}^1$ at +0.79 V of $[\mathbf{1}]^+$ was assigned to $[\mathbf{1}]^{2+}$/$[\mathbf{1}]^+$ couple. The reversible cathodic wave with $E_{½}^2$ at −0.66 V (ΔE=120 mV) of $[\mathbf{1}]^+$ was assigned to $[\mathbf{1}]^+$/$[\mathbf{1}]^\bullet$ couple. The electrogenerated paramagnetic reduced $[\mathbf{1}]^\bullet$ radical was analyzed by UV–vis, EPR spectra and unrestricted DFT calculations.

The conversion of $[\mathbf{1}]^+ \rightarrow [\mathbf{1}]^\bullet$ in CH_2Cl_2 was investigated by spectroelectrochemical measurement at 25 °C. The change of UV–vis spectral features is illustrated in Fig. 2b. It is observed that during the reduction, the intensity of both the lower energy absorption bands gradually decreases.

The EPR spectrum of the CH_2Cl_2 frozen glass of the electrogenerated $[\mathbf{1}]^\bullet$ was recorded at 25 °C. The EPR spectrum is depicted in Fig. 2c. The *g* value, 2.003 is consistent with the formation of $[\mathbf{1}]^\bullet$ radical. The hyperfine splitting due to ^{14}N nucleus affirm the localization of the spin density on the pyrazine heterocycle (*vide infra*).

Gas Phase Geometries and Electronic Structures of $[\mathbf{1}]^+$ and $[\mathbf{1}]^\bullet$

The geometries of $[\mathbf{1}]^+$ and $[\mathbf{1}]^\bullet$ in gas phase were optimized respectively with singlet and doublet spin states at the B3LYP/DFT level. The calculated bond parameters of $[\mathbf{1}]^+$ and $[\mathbf{1}]^\bullet$ are summarized in Table 2. The optimized geometry of $[\mathbf{1}]^+$ and the Mulliken spin density plot of $[\mathbf{1}]^\bullet$ are shown in the Fig. 3. Atomic spin populations are listed under the caption of the Fig. 3. Mulliken spin population analysis reveals that the unpaired electron is primarily localized on the phenyl substituted pyrazine ring which corroborates well with EPR spectrum of $[\mathbf{1}]^\bullet$ radical (Fig. 2c).

The origin of the lower energy excitation of the $[\mathbf{1}]^+$ ion was elucidated by the time dependent (TD) DFT calculation. Excitation energies (λ/nm) of the transitions with the oscillator strengths (*f*) greater than 0.02 of UV–vis absorption bands of $[\mathbf{1}]^+$ ion are listed in Table S1. The calculated spectra of $[\mathbf{1}]^+$ ion is illustrated in Fig. S1. The photoactive orbitals are shown in Fig. 4. Analyse show that the absorption maxima at 410 nm is due to the $\pi \rightarrow \pi^*$ transition.

Table 2 Selected calculated bond parameters of $[\mathbf{1}]^+$ and $[\mathbf{1}]^\bullet$

	$[1]^+$	$[1]^\bullet$
C17-C18	1.4613	1.4299
C18-N29	1.3384	1.3869
N29-C22	1.4017	1.4089
C22-C21	1.4325	1.4304
C21-N30	1.3675	1.3879
N30-C17	1.3056	1.3175
N29-C32	1.4586	1.4375

DNA Intercalation and Spectral Features

A series of experiments were performed to determine the propensity of this compound to bind to DNA.

UV–vis Spectra

The absorption maximum of [**1**][Cl] at around 338 nm is convenient to monitor its interaction with DNA. Addition of DNA to the cation resulted in hypochromic effect and bathochromic shift which are observed due the overlap of the π electron cloud of [**1**][Cl] with that of the base pairs indicating a strong intermolecular association (Fig. 5a).

The presence of two sharp isosbestic points at 349 and 373 nm revealed the presence of two state system consisting of bound and free [**1**][Cl] enabling application of equilibrium conditions in the complexation process. The λ_{max} of free and DNA bound [**1**][Cl] were 338 and 345 nm, respectively, ε_f= 53400 $M^{-1}cm^{-1}$ (338 nm), ε_B=28897 $M^{-1}cm^{-1}$ (345 nm) and ε_{iso}=28493 $M^{-1}cm^{-1}$ (at 349 nm). Titrations of a constant concentration of [**1**][Cl] with several inputs of DNA was carried out subsequently and the data were used to construct a Scatchard plot of r/C_f vs. r, where r is the number of moles of [**1**][Cl] cation bound per mole of DNA base pairs. The Scatchard plot, in the inset of Fig. 5a, clearly reveals that at low values of r there is negative slope indicating the non-cooperative binding enabling the fitting of the curves to a theoretical curve drawn according to the excluded site model of McGhee and von Hippel [34] for non-cooperative binding system to derive the best-fit parameters of the intrinsic binding constant (K_i=5.39×10^4 M^{-1}) to an isolated binding site and the number of base pairs (n=2.05) excluded by the binding of a single [**1**][Cl] cation.

Fluorescence Spectra

Fluorescence quenching study was performed to further substantiate the presumably intercalative DNA binding mode of [**1**][Cl]. The relative fluorescence intensity decrease of [**1**][Cl] upon addition of DNA is shown in the Fig. 5b. The results showed clearly that with the increasing concentration of DNA

the fluorescence intensity decreased steadily. So the cationic [**1**][Cl] is a very effective binder of DNA.

Circular Dichroism (CD) Spectra

[**1**][Cl] is an optically inactive molecule and hence we used circular dichroism to further understand the interaction phenomenon. The CD spectrum of DNA is characterised by positive and negative bands around 278 and 245 nm, respectively, which represents a typical B-form structure. These CD bands of the double helical DNA arise from a combination of stacking interactions between the base pairs and the helical structure that provide asymmetric environment for the bases [37]. Figure 6a depicts the CD spectra of DNA in the absence and in the presence of increasing concentrations of [**1**][Cl] in 200–400 nm region. Both the bands were perturbed in the presence of increasing concentrations of [**1**][Cl] resulting in a increase of the 278 nm band ellipticity and a concomitant increase of the 245 nm band intensity. The band ellipticity change of the 245 negative band was smaller compared to that of the 278 nm. The increase in the molar ellipticity of 278 nm band generally occurs when small molecules stack between the base pairs of DNA i.e., during intercalative binding because groove binding of small molecules does not result in unwinding of DNA base pairs and thereby does not cause an increase of molar ellipticity of 278 nm band on addition. Therefore, the mode of binding of [**1**][Cl] to DNA can be inferred to be of intercalative kind.

Optical Melting

The binding of [**1**][Cl] to the DNA was also evaluated from optical thermal melting studies [33]. Double stranded CT DNA under the conditions of the experiment melted with a T_m value of 78.3 °C. The melting temperature of the DNA was enhanced on binding of [**1**][Cl] to around 84.8 °C. Thus a ΔT_m value of about 6.5 °C was observed on [**1**][Cl] binding. Such a high stabilization of the DNA helix appears to be due to the strong binding of [**1**][Cl] to the duplex DNA. The optical melting profiles of DNA and its complex at saturation with [**1**][Cl] is presented in Fig. 6b.

Gel-Electrophoresis Studies

The results of interaction between DNA (pUC19) and [**1**][Cl] as analysed by gel electrophoresis are shown in the Fig. 7. Lane 4 in upper panel **a** evidenced pUC19 DNA control with two bands, extremely faint upper [Nicked Circular (NC)] and strong lower one [Supercoiled (SC)].

The comparison of DNA band intensity is given in the lower panel **a**. The change in band intensity indicated the formation NC from SC as a consequence of binding with cation $[\mathbf{1}]^+$ containing complex.

It is evident from the figure that the interaction of higher concentrations of cation $[\mathbf{1}]^+$ resulted lowering the intensity of SC while increasing that of NC (lower panel **a**). Here the NC state was retarded one due to size increase by nicking upon interaction with cation $[\mathbf{1}]^+$ and such change in molecular size was dependent on the concentration (4, 6 and 8 mM). Also, it is to be noted that both NC and SC bands have shown slight retardation compared to control due to probable binding of the drug with DNA. It is well established that the interaction of EB with DNA, result gel band mobility retardation. EB is a very strong DNA intercalating agent giving alteration of molecular size and conformation of DNA due to intercalation [38].

The compound under study exhibited marked mobility shift of DNA bands from SC to NC as reported in case of EB. Further its intercalating property is strongly supported from the change in CD spectra after its binding with DNA (Fig. 6a).

Panel **b** of Fig. 7 shows gel electrophoresis study on the interaction of CT DNA with varying concentrations (4, 6 and 8 mM) of [**1**][Cl]. As evident from the panel **b** of Fig. 7, compared to the control in lane 1, all the other lanes displayed DNA gel band retardation. CT DNA is a huge large molecule and binding to small cationic complex [**1**][Cl] did not affect much of its gel mobility, hence the change in mobility retardation was indicative only.

Hydrodynamic Studies

To confirm intercalation, we also exploited the changes in length and stiffening of rod like structure of the sonicated DNA on [**1**][Cl] binding that is a diagnostic test in establishing the binding mode to DNA [36, 39]. The hydrodynamic behaviour of the DNA as measured by viscosity change of the complex is explored for this purpose. The results of viscosity increase with increasing amounts of the [**1**][Cl] is shown in the Fig. 7c which clearly reveals a sharp rise in viscosity which attained a plateau indicating a maximum enhancement of the frictional resistance or change in the shape of DNA on binding due to intercalation of [**1**][Cl] cation between the base pairs of DNA.

Thermodynamic Characterization

Finally, thermodynamic characterization of the DNA binding of [**1**][Cl] was performed by highly sensitive isothermal titration calorimetry (ITC). ITC is a technique that can provide detailed information about standard molar Gibbs energy, enthalpy of binding, the entropy contribution along with the equilibrium binding constant and stoichiometry [40]. Upper panel of Fig. 8 shows the representative raw heat profile resulting from a typical ITC experiment in which DNA was titrated from the syringe into [**1**][Cl] solution in the

calorimetric cell. The titration resulted in a single exothermic binding event enabling the data to be fitted to a single set of identical binding sites model (lower panel of Fig. 8).

To extract the binding and thermodynamic parameters of the interaction, the thermogram was fitted to a single site model and the thermodynamic parameters were estimated from the best fit to the observed heat release. The data were analyzed with several different initial guesses and the resulting fits gave consistent values of the parameters, $K_a = 5.30 \pm 0.12 \times 10^4\ M^{-1}$, $\Delta H^o = -0.590 \pm 0.40$ kcal/mol, a $T\Delta S^o$ of 5.84 kcal/mol and a binding site size of ~2.0 base pairs. The binding affinity value obtained from ITC analysis was in good agreement with that obtained from the McGhee-von Hippel analysis of the absorbance data. The binding standard molar Gibbs energy change (ΔG^o) was −6.43 kcal/mol. The large entropy term and relatively small enthalpy term suggested that the binding of [**1**][Cl] to DNA is predominantly entropy driven [41–43]. This strong positive entropy term appears to be due to the disruption and release of DNA-bound water molecules and the negative enthalpy term, although small, originates from non-covalent stacking interaction from intercalation binding.

Conclusions

In summary, we report the synthesis of 7-phenylacenaphtho [1,2-*b*]quinoxalin-7-ium chloride, [**1**][Cl], a new fluorescent molecule. $[\mathbf{1}]^+$ ion which is redox active and upon reduction at −0.66 V affords the radical analogue $[\mathbf{1}]^{\bullet}$ authenticated by UV–vis, EPR spectra and DFT calculation. TD DFT calculation established that the emissive excitation of $[\mathbf{1}]^+$ ion at 410 nm is due to the $\pi \rightarrow \pi^*$ transition. $[\mathbf{1}]^+$ ion is a strong DNA intercalator that may be useful as DNA targeted small drug molecule.

Acknowledgments Financial support received from DBT (No. BT/PR13754/Med/29/181/2010) and DST (SR/S1/IC/0026/2012), New Delhi, India are gratefully acknowledged. SK and AYK are thankful to Council of Scientific and Industrial Research and University Grants Commission respectively, for fellowships. AB was an INSPIRE fellow of DST.

References

1. Benner K, Ihmels H, Kölsch S, Pithan PM (2014) Targeting a basic site-containing DNA with annelated quinolizinium derivatives: the influence of size, shape and substituents. Org Biomol Chem 12: 1725–1734
2. Singh M, Sur S, Rastogi GK, Jayaram B, Tandon V (2013) Bi and tri-substituted phenyl rings containing bisbenzimidazoles bind differentially with DNA duplexes: a biophysical and molecular simulation study. Mol BioSyst 9:2541–2553
3. Jia T, Xiang J, Wang J, Guo P, Yu J (2013) Interactions of newly designed dicationic carbazole derivatives with double-stranded DNA: syntheses, binding studies and AFM imaging. Org Biomol Chem 11:5512–5520
4. Bhadra K, Kumar GS (2011) Interaction of berberine, palmatine, coralyne, and sanguinarine to quadruplex DNA: a comparative spectroscopic and calorimetric study. Biochim Biophys Acta Gen Subj 1810:485–496
5. Phillips T, Haq I, Thomas JA (2011) Water-soluble amino derivatives of free-base dppz- syntheses and DNA binding studies. Org Biomol Chem 9:3462–3470
6. Shewach DS, Kuchta RD (2009) Introduction to cancer chemotherapeutics. Chem Rev 109:2859–2861
7. Wilhelmsson LM, Kingi N, Bergman J (2008) Interactions of antiviral Indolo[2,3-b]quinoxaline derivatives with DNA. J Med Chem 51:7744–7750
8. Phillips T, Rajput C, Twyman L, Haq I, Thomas JA (2005) Water-soluble organic dppz analogues-tuning DNA binding affinities, luminescence, and photo-redox properties. Chem. Commun. 4327–4329
9. Phillips T, Haq I, Meijer AJHM, Adams H, Soutar I, Swanson L, Sykes MJ, Thomas JA (2004) DNA binding of an organic dppz-based intercalator. Biochemistry 43:13657–13665
10. Hurley LH (2002) DNA and its associated processes as targets for cancer therapy. Nat Rev Cancer 2:188–200
11. García-Nieto R, Manzanares I, Cuevas C, Gago F (2000) Increased DNA binding specificity for antitumor ecteinascidin 743 through Protein-DNA interactions? J Med Chem 43:4367–4369
12. Lippert B (1999) In: Chemistry and biochemistry of a leading anticancer drug. Wiley-VCH, Weinheim, Germany
13. Sinan M, Panda M, Ghosh A, Dhara K, Fanwick PE, Chattopadhyay DJ, Goswami S (2008) Mild synthesis of a family of planar triazinium cations via proton-assisted cyclization of pyridyl containing Azo compounds and studies on DNA intercalation. J Am Chem Soc 130:5185–5193
14. Clark ML, Green RL, Johnson OE, Fanwick PE, McMillin DR (2008) DNA-binding and physical studies of Pt(4′-NR_2-trpy)CN^+ systems (trpy = 2,2′:6′,2″-terpyridine). Inorg Chem 47:9410–9418
15. Kundu S, Biswas MK, Banerjee A, Bhadra K, Kumar GS, Drew MGB, Bhadra R, Ghosh P (2013) Synthesis, structure and DNA binding studies of 9-phenyldibenzo[a, c] phenazin-9-ium. RSC Adv 3:3054–3061
16. Frisch MJ, Trucks GW, Schlegel HB, Scuseria GE, Robb MA, Cheeseman JR, Montgomery JA Jr, Vreven T, Kudin KN, Burant JC, Millam JM, Iyengar SS, Tomasi J, Barone V, Mennucci B, Cossi M, Scalmani G, Rega N, Petersson GA, Nakatsuji H, Hada M, Ehara M, Toyota K, Fukuda R, Hasegawa J, Ishida M, Nakajima T, Honda Y, Kitao O, Nakai H, Klene M, Li X, Knox JE, Hratchian HP, Cross JB, Bakken V, Adamo C, Jaramillo J, Gomperts R, Stratmann RE, Yazyev O, Austin JA, Cammi R, Pomelli C, Ochterski JW, Ayala PY, Morokuma K, Voth GA, Salvador P, Dannenberg JJ, Zakrzewski VG, Dapprich S, Daniels AD, Strain MC, Farkas O, Malick DK, Rabuck AD, Raghavachari K, Foresman JB, Ortiz JV, Cui Q, Baboul AG, Clifford S, Cioslowski J, Stefanov BB, Liu G, Liashenko A, Piskorz P, Komaromi I, Martin RL, Fox DJ, Keith T, Al-Laham MA, Peng CY, Nanayakkara A, Challacombe M, Gill PMW, Johnson B, Chen W, Wong MW, Gonzalez C, Pople JA (2004) *Gaussian 03, revision E.01*. Gaussian, Inc., Wallingford, CT
17. Parr RG, Yang W (1989) Density functional theory of atoms and molecules. Oxford University Press, Oxford, U.K.
18. Salahub DR, Zerner MC (1989) The challenge of d and f electrons; ACS symposium series 394. American Chemical Society, Washington, DC
19. Kohn W, Sham L (1965) Self-consistent equations including exchange and correlation effects. J Phys Rev A 140:1133–1138
20. Hohenberg P, Kohn W (1964) Inhomogeneous electron gas. Phys Rev B 136:864–871

21. Stratmann RE, Scuseria GE, Frisch M (1998) An efficient implementation of time-dependent density-functional theory for the calculation of excitation energies of large molecules. J Chem Phys 109:8218–8224
22. Casida ME, Jamoroski C, Casida KC, Salahub DR (1998) Molecular excitation energies to high-lying bound states from time-dependent density-functional response theory: characterization and correction of the time-dependent local density approximation ionization threshold. J Chem Phys 108:4439–4449
23. Bauernschmitt R, Haser M, Treutler O, Ahlrichs R (1996) Treatment of electronic excitations within the adiabatic approximation of time dependent density functional theory. Chem Phys Lett 454:454–464
24. Becke AD (1993) Density-functional thermochemistry. III. The role of exact exchange. J Chem Phys 98:5648–5651
25. Miehlich B, Savin A, Stoll H, Preuss H (1989) Results obtained with the correlation energy density functionals of becke and Lee, Yang and Par. Chem Phys Lett 157:200–206
26. Lee C, Yang W, Parr RG (1988) Development of the Colle-Salvetti correlation-energy formula into a functional of the electron density. Phys Rev B 37:785–789
27. Pulay P (1982) Improved SCF convergence acceleration. J Comput Chem 3:556–560
28. Schlegel HB, McDouall JJ (1991) In: Ogretir C, Csizmadia IG (eds) Computational advances in organic chemistry. Kluwer, The Netherlands, pp 167–185
29. Petersson GA, Al-Laham MA (1991) A complete basis set model chemistry. II. Open-shell systems and the total energies of the first-row atoms. J Chem Phys 94:6081–6090
30. Petersson GA, Bennett A, Tensfeldt TG, Al-Laham MA, Shirley WA, Mantzaris J (1988) A complete basis set model chemistry. I. The total energies of closed-shell atoms and hydrides of the first-row elements. J Chem Phys 89:2193–2218
31. Cossi M, Rega N, Scalmani G, Barone V (2003) Energies, structures, and electronic properties of molecules in solution with the C-PCM solvation model. J Comput Chem 24:669–681
32. Barone V, Cossi M (1998) Quantum calculation of molecular energies and energy gradients in solution by a conductor solvent model. J Phys Chem A 102:1995–2001
33. Sinha R, Kumar GS (2009) Interaction of isoquinoline alkaloids with an RNA triplex: structural and thermodynamic studies of berberine, palmatine, and coralyne binding to Poly(U). Poly(A)*Poly(U). J Phys Chem B 113:13410–13420
34. McGhee JD, von Hippel PH (1974) Theoretical aspects of DNA-protein interactions: co-operative and non-co-operative binding of large ligands to a one-dimensional homogeneous lattice. J Mol Biol 86:469–489
35. Sinha R, Hossain M, Kumar GS (2007) RNA targeting by DNA binding drugs: Structural, conformational and energetic aspects of the binding of quinacrine and DAPI to A-form and H^L-form of poly(rC)·poly(rG). Biochim Biophys Acta Gen Subj 1770:1636–1650
36. Satyanarayana S, Dabrowiak JC, Chaires JB (1992) Neither Δ- nor Λ-Tris(phenanthroline)ruthenium(II) binds to DNA by classical interaction. Biochemistry 31:9319–9324
37. Rajendran A, Nair BU (2006) Unprecedented dual binding behaviour of acridine group of dye: a combined experimental and theoretical investigation for the development of anticancer chemotherapeutic agents. Biochim Biophys Acta Gen Subj 1760:1794–1801
38. Sigmon J, Larcom LL (1996) The effect of ethidium bromide on mobility of DNA fragments in agarose gel electrophoresis. Electrophoresis 17:1524–1527
39. Sinha R, Islam MM, Bhadra K, Kumar GS, Banerjee A, Maiti M (2006) The binding of DNA intercalating and non-intercalating compounds to A-form and protonated form of poly(rC)·poly(rG): Spectroscopic and viscometric study. Bioorg Med Chem 14:800–814
40. Bhadra K, Kumar GS (2010) Isoquinoline alkaloids and their binding with DNA: calorimetry and thermal analysis applications. Mini-Rev Med Chem 10:1235–1247
41. Das A, Kumar GS (2012) Drug-DNA binding thermodynamics: a comparative study of aristololactam-β-d-glucoside and daunomycin. J Chem Thermodyn 54:421–428
42. Chowdhury SR, Islam MM, Kumar GS (2010) Binding of the anticancer alkaloid sanguinarine to double stranded RNAs: insights into the structural and energetics aspects. Mol BioSyst 6:1265–1276
43. Adhikari A, Hossain M, Maiti M, Kumar GS (2008) Energetics of the binding of phototoxic and cytotoxic plant alkaloid sanguinarine to DNA: isothermal titration calorimetric studies. J Mol Struct 889:54–63